Electronic Supplementary Material (ESI) for Physical Chemistry Chemical Physics.

Supplementary Information

Assembly and Relaxation Behaviors of Phosphatidylethanolamine Monolayers Investigated by Polarization and Frequency Resolved SFG-VS

*Feng Wei**[†], Wei Xiong, Wenhui Li, Wangting Lu, Heather C. Allen, Wanquan Zheng*

1. Experimental details of π-A isotherm and BAM detections

Three PE lipids: DMPE, D_{54}-DMPE and DPPE (Avanti lipids, purity> 99%) were analyzed in this study. The lipid solutions for spreading were prepared using the mixing solute of $CHCl_3$: Methanol = 4:1. For each isotherm experiments, about 35 ul lipid solution (1 mM) were spread on the surface of deionize water (Milli-Q Academic). The Langmuir isotherm of DMPE and DPPE monolayers were collected by KSV Teflon mini Trough with a compression speed of 5mm/min. The same Langmuir trough was also used in SFG-VS detection to control the SP of monolayer. For SFG spectra collection at stabilized SP value (± 0.3 mN/m), the compression speed of ± 3 mm/min was used. For the compression kinetics detection, the compression speed was 27 mm/min.

BAM images of the monolayers were collected simultaneously with π-A isotherms using a custom-built BAM. The laser source (Research Electro-Optics) emits 5 mW p-polarized light at 543 nm. The incident beam is first attenuated by a half-wave plate and then filtered by a Glan-Thompson polarizer before reaching the aqueous surface at the Brewster angle (~53°). The reflected beam is collected by an infinity-corrected Nikon 10° objective lens and is then focused by a tube lens. A back-illuminated electron multiplying CCD camera (Andor, model DV887-BV, 512 × 512 pixels) was used to record BAM images. The inclined position of the imaging optics

results in images focused along a central narrow stripe. Final images taken were cropped from a 800 μm × 800 μm size to show the most resolved regions, which was typically the center of the image where the beam was the most intense.

2. SFG spectra of ODT monolayers

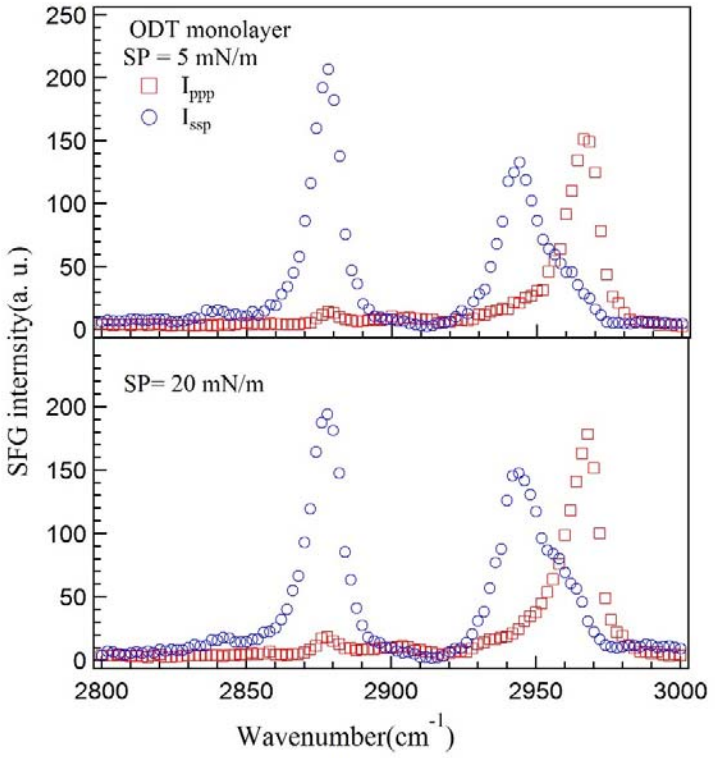

Figure S1. SFG spectra of ODT monolayer at SP = 5 mN/m and 20 mN/m in the wavenumber range of 2800-3000 cm^{-1}.

3. Fitting of SFG-VS Signals

As described in detail elsewhere, the intensity of the SFG light is proportional to the square of the sample's effective second-order nonlinear susceptibility($\chi_{eff}^{(2)}$), and the intensity of the two input fields $I_1(\omega_{vis})$ and $I_2(\omega_{IR})$, see eq. (S1), which vanishes when a material has inversion symmetry.[1-7]

$$I(\omega_{SFG}) \propto \left|\chi_{eff}^{(2)}\right|^2 I_1(\omega_{vis}) I_2(\omega_{IR}) \qquad \text{(S1)}$$

where $\omega_{SFG} = \omega_{IR} + \omega_{vis}$. As the IR beam frequency is tuned over the vibrational resonance of surface/interface molecules, the effective surface nonlinear susceptibility $\chi_R^{(2)}$ can be enhanced. The frequency dependence of $\chi_{eff}^{(2)}$ is described by eq. (S2)

$$\chi_{eff}^{(2)}(\omega) = \chi_{NR}^{(2)} + \sum_{\upsilon} \frac{A_\upsilon}{\omega - \omega_\upsilon + i\Gamma_\upsilon} \qquad \text{(S2)}$$

where A_υ, ω_υ, and Γ_υ are the strength, resonant frequency, and damping coefficient of the vibrational mode(ν), respectively. A_υ could be either positive or negative depending on the phase of the vibrational mode. The plot of SFG signal vs. the IR input frequency shows a polarized vibrational spectrum of the molecules at surface or interface. A_υ, ω_υ, and Γ_υ can be extracted by fitting the spectrum. The fitting parameters of SFG spectra of DMPE monolayer at 3mN/m and 20 mN/m are listed in table S1 for demonstration.

Table S1 Fitting parameters of SFG spectra of DMPE monolayer at 3mN/m and 20 mN/m

SP		3 mN/m		20 mN/m	
Polarization		PPP	SSP	PPP	SSP
A_0		0.65 ± 0.09	0.54 ± 0.09	-0.39 ± 0.07	-0.74 ± 0.29
Peak 1	A	-32.07 ± 16.23	10.29 ± 7.66		
	ω_0	2837.1 ± 2.4			
	Γ	16.9 ± 5.8			
Peak 2	A	-18.63 ± 4.87	-33.24 ± 2.19	14.87±1.22	13.98 ± 1.47
	ω_0	2855.0 ± 0.4		2848.5 ± 0.9	
	Γ	7.6 ± 0.4		8.4 ± 0.6	
Peak 3	A	9.79 ± 1.51	-38.41 ± 1.84	-18.92 ± 2.09	110.93 ± 2.23
	ω_0	2882.1 ± 0.2		2880.8 ± 0.1	
	Γ	4.9 ± 0.2		6.2 ± 0.1	
Peak 4	A	-2.69 ± 1.98	-5.34 ± 2.45	-24.22 ± 5.85	31.27 ± 6.70
	ω_0	2930.2 ± 0.8		2901.6 ± 0.7	

	Γ	4.7 ± 1.8		10.2 ± 1.7	
	A	2.44 ± 2.04	-53.81 ± 3.58	-25.10 ± 2.73	120.95 ± 3.79
Peak 5	ω_0	2947.1 ± 0.4		2943.4 ± 0.2	
	Γ	7.8 ± 0.4		9.0 ± 0.2	
	A	5.50 ± 1.70	-5.93 ± 2.33	-18.36 ± 5.16	7.09 ± 2.89
Peak 6	ω_0	2957.8 ± 0.3		2957.2 ± 0.4	
	Γ	3.7 ± 0.8		5.6 ± 1.0	
	A	-37.50 ± 1.54	2.87 ± 1.31	74.23 ± 1.82	-15.83 ± 1.91
Peak 7	ω_0	2970.4 ± 0.2		2970.1 ± 0.2	
	Γ	4.4 ± 0.2		5.1 ± 0.1	
C_0		4.67 ± 0.42	1.25 ± 0.99	4.89 ± 1.1	-4.85 ± 1.21

4. Tilt angle analysis

The molecular orientation information can be obtained by relating SFG susceptibility tensor elements $\chi_{ijk}(i,j,k=x,y,z)$ to the SFG molecular hyperpolarizability tensor elements $\beta_{lmn}(l,m,n=a,b,c)$.[4-6] The components of $\chi_{eff}^{(2)}$ of ssp, and ppp polarization combinations are given in equations (S5)-(S6) in the lab coordinate system which is defined as the z-axis being along the surface normal and the x-axis being in the incident plane.[4-6]

$$\chi_{eff,ssp}^{(2)} = L_{yy}(\omega_{SF})L_{yy}(\omega_{Vis})L_{zz}(\omega_{IR})\sin\beta_{IR}\chi_{yyz}^{(2)} \qquad \text{(S3)}$$

$$\begin{aligned}\chi_{eff,ppp}^{(2)} = &-L_{xx}(\omega_{SF})L_{xx}(\omega_{Vis})L_{zz}(\omega_{IR})\cos\beta_{SF}\cos\beta_{Vis}\sin\beta_{IR}\chi_{xxz}^{(2)}\\ &-L_{xx}(\omega_{SF})L_{zz}(\omega_{Vis})L_{xx}(\omega_{IR})\cos\beta_{SF}\sin\beta_{Vis}\cos\beta_{IR}\chi_{xzx}^{(2)}\\ &+L_{zz}(\omega_{SF})L_{xx}(\omega_{Vis})L_{xx}(\omega_{IR})\sin\beta_{SF}\cos\beta_{Vis}\cos\beta_{IR}\chi_{zxx}^{(2)}\\ &+L_{zz}(\omega_{SF})L_{zz}(\omega_{Vis})L_{zz}(\omega_{IR})\sin\beta_{SF}\sin\beta_{Vis}\sin\beta_{IR}\chi_{zzz}^{(2)}\end{aligned} \qquad \text{(S4)}$$

where β_{SF}, β_{Vis} and β_{IR} are the angles between the surface normal and the sum frequency beam, the input visible beam, and the input IR beam, respectively. L_{ii} (i = x, y or z) denotes the Fresnel coefficients. Under current experimental geometry, after considering the Fresnel coefficient constants, eqs.(S5-S6) are then given by

CH_3 groups:

$$\chi_{eff,ssp}^{(2)} = 0.249\chi_{yyz}^{(2)} \qquad \text{(S5)}$$

$$\chi^{(2)}_{eff,ppp} = \text{-}0.159\chi^{(2)}_{xxz} + 0.226\chi^{(2)}_{zzz} \quad \text{(S6)}$$

PO_2^- groups:

$$\chi^{(2)}_{eff,ssp} = 0.244\chi^{(2)}_{yyz} \quad \text{(S7)}$$

$$\chi^{(2)}_{eff,ppp} = \text{-}0.156\chi^{(2)}_{xxz} + 0.225\chi^{(2)}_{zzz} \quad \text{(S8)}$$

3.1. CH_3 groups.

Here we treated CH_3 groups as C_{3v} symmetry The SFG susceptibility tensor elements $\chi_{ijk}(i,j,k=x,y,z)$ of $C_{\infty v}$ symmetry have following relationships.[4-6]

$$\chi^{(2)}_{xxz,ss} = \chi^{(2)}_{yyz,ss} = \frac{1}{2}N_s\beta_{ccc}[(1+R)\langle\cos\theta\rangle - (1-R)\langle\cos^3\theta\rangle] \quad \text{(S9)}$$

$$\chi^{(2)}_{zzz,ss} = N_s\beta_{ccc}[R\langle\cos\theta\rangle + (1-R)\langle\cos^3\theta\rangle] \quad \text{(S10)}$$

$$R = \frac{1+r-(1-r)\cos^2\tau}{2(r+(1-r)\cos^2\tau)} \quad \text{(S11)}$$

$$\chi^{(2)}_{xxz,as} = \chi^{(2)}_{yyz,as} = -N_s R'\beta_{ccc}(\langle\cos\theta\rangle - \langle\cos^3\theta\rangle) \quad \text{(S11)}$$

$$\chi^{(2)}_{zzz,ss} = 2N_s R'\beta_{ccc}[\langle\cos\theta\rangle - \langle\cos^3\theta\rangle] \quad \text{(S12)}$$

$$R' = \frac{\beta_{aca}}{\beta_{ccc}} = \frac{-(1-r)\sin^2\tau\dfrac{G_{as}}{\omega_{as}}}{2(r+(1-r)\cos^2\tau)\dfrac{G_{ss}}{\omega_{ss}}} \quad \text{(S13)}$$

The parameter R is estimated to be 3.338 when r = 0.03 and $\tau = 109.5°$, and the parameter R' is estimated to be 2.80.[7] By substitution of eqs. (S9)-(S10) in eqs.(S7)-(S8), the deduced susceptibility ratio $\chi^{(2)}_{ssp,CH_3-ss} / \chi^{(2)}_{ssp,CH_3-as}$ can be plotted as a function of orientation angle (θ) (shown in Figure S2).

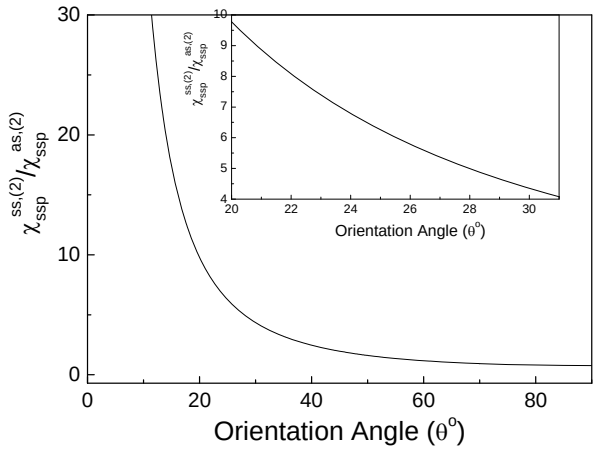

Figure S2 Deduced susceptibility ratio of $\chi^{(2)}_{ssp,\mathrm{CH_3}-ss}$ / $\chi^{(2)}_{ssp,\mathrm{CH_3}-as}$ is plotted as a function of orientation angle (θ) for the CH_3 groups which was treated as having C_{3v} symmetry.

3.2. PO_2^- groups.

The symmetry of PO_2^- group can be treated as C_{2v} symmetry. The peaks at ~ 1100 cm^{-1} can be assigned to A_1 modes.[8-10] The susceptibility tensor elements of A_1 mode in C_{2v} symmetry are described as following equations.[4-6]

A_1 mode:

$$\chi^{(2),A1}_{xxz} = \chi^{(2),A1}_{yyz} = \frac{1}{2}N_s\beta_{ccc}[\langle\cos^2\psi\rangle R_a + \langle\sin^2\psi\rangle R_b + 1]\langle\cos\theta\rangle + \frac{1}{2}N_s\beta_{ccc}[\langle\sin^2\psi\rangle R_a + \langle\cos^2\psi\rangle R_b - 1]\langle\cos^3\theta\rangle \quad \text{(S14)}$$

$$\chi^{(2),A1}_{zzz} = N_s\beta_{ccc}[\langle\sin^2\psi\rangle R_a + \langle\cos^2\psi\rangle R_b]\langle\cos\theta\rangle - N_s\beta_{ccc}[\langle\sin^2\psi\rangle R_a + \langle\cos^2\psi\rangle R_b - 1]\langle\cos^3\theta\rangle \quad \text{(S15)}$$

where ψ is the twisting angle of PO_2^- group. Using the bond polarizability derivative model, the polarization ratios of R_a and R_b of $O\cdots P\cdots O$ stretch in pyridine ring is determined by taking $r_{P\text{-}O}$ = 0.54(corresponding Raman depolarization ration is 0.33) and τ=120°.[11]

$$R_a = \frac{\beta_{aac}}{\beta_{ccc}} = \frac{1 + r - (1 - r)\cos\tau}{1 + r + (1 - r)\cos\tau} \quad \text{(S16)}$$

$$R_b = \frac{\beta_{bbc}}{\beta_{ccc}} = \frac{2r}{1+r+(1-r)\cos\tau} \qquad \text{(S17)}$$

According to eqs.(S16) and (S17), the deduced susceptibility ratio $\chi^{(2)}_{ppp,PO_2^-\text{-}ss} / \chi^{(2)}_{ssp,PO_2^-\text{-}ss}$ at $\psi = 0°$ can be plotted as a function of the tilt angle (shown in Figure S3).

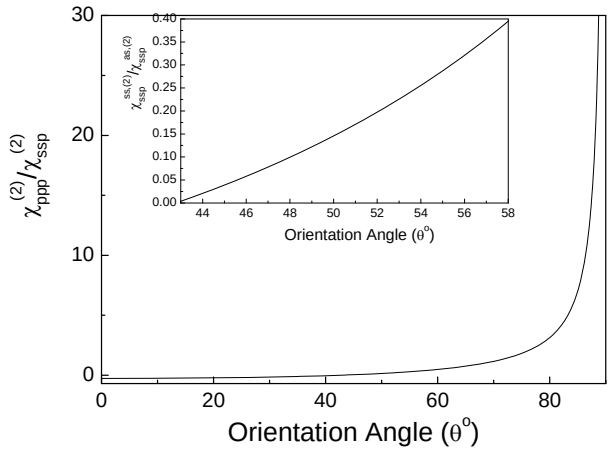

Figure S3 The deduced susceptibility ratio $\chi^{(2)}_{ppp,PO_2^-\text{-}ss} / \chi^{(2)}_{ssp,PO_2^-\text{-}ss}$ is plotted as a function of the tilt angles of PO_2^- group treating $O \doteq P \doteq O$ bond as having C_{2v} symmetry.

5. $R^{1105\text{cm}^{-1}}$ and $R^{2970\text{cm}^{-1}}$ of DMPE and DPPE monolayers

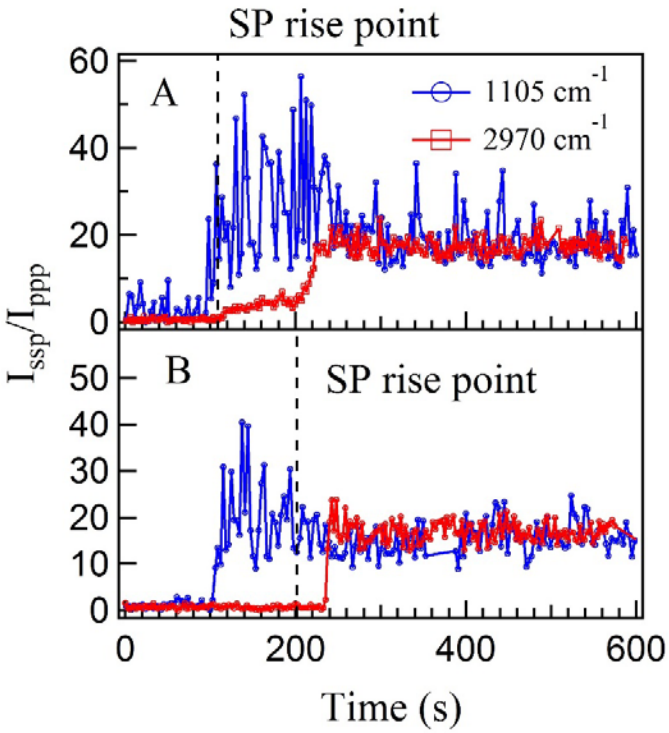

Figure S4. $R^{1105\text{cm}^{-1}}$ and $R^{2970\text{cm}^{-1}}$ of A). DMPE and B). DPPE monolayers during the compression

References

1. Antonov L.; Nedeltcheva, D. *Chem. Soc. Rev.,* **2000**, 29, 217–227.

2. Crisponi, G. *React. Funct.l Polym.,* **1997**, 34, 121-126.

3. Ghasemi, J.; Niazi, A.; Kubista M.; Elbergali, A. *Analyt. Chim. Acta,* **2002**, 455, 335–342.

4. Shen, Y. R. The Principles of Nonlinear Optics; John Wiley& Sons: New York, **1984**.

5. Lambert, A. G.; Davies P. B.; Neivandt, D. J *Appl. Spectrosc. Rev.,* **2005**, 40, 103–145.

6. Wang, H. F.; Gan, W.; Lu, R.; Rao, Y.; Wu, B. H. *Int. Rev. Phys. Chem.* **2005**, 24, 191–256.

7. Biswas N.; Umapathy, S.; *J. Chem. Phys.,* **1997**, 107, 7849-7858.

8. Castellucci, E.; Sbrana G.; Verderame, F. D. *J. Chem. Phys.,* **1969**, 51, 3762-3770.

9. Moskovits, M.; DiLella D. P.; Maynard, K. J. *Langmuir,* **1988**, 4, 61-76.

10. Golab, J. T.; Sprague, J. R.; Carron, K. T.; Schatz G. C.; Van Duyne, R. P. *J. Chem. Phys.,* **1988**, 88, 7942-7951.
11. Chen, C. Y.; Liu, W. T.; Pagliusi, P.; Shen, Y. R. *Macromolecules,* **2009**, 42, 2122-2126.